The 8th European Congress on Computational Methods in Applied Sciences and Engineering
ECCOMAS Congress 2022
5 – 9 June 2022, Oslo, Norway

STOCHASTIC SIMULATION OF THE HEAD IMPACT ON WINDSCREENS

C. BROKMANN*, C. ALTER* AND S. KOLLING*

* Institute of Mechanics and Materials, THM University of Applied Sciences, Wiesenstrasse 14, D-35390 Giessen, Germany
e-mail: stefan.kolling@me.thm.de, https://www.thm.de/site/en/

Key words: Crash and Impact, Stochastic Simulation, Fracture of Glass.

Abstract. In accidents involving cars with pedestrians, the impact of the head on structural parts of the vehicle takes a significant risk of injury. If the head hits the windscreen, the injury is highly influenced by glass fracture.

In pedestrian protection tests, a head impactor is shot on the windscreen while the resultant acceleration at the COG of the head is measured. To assess the risk of fatal or serious injury, a head injury criterion (HIC) as an explicit function of the measured acceleration can be determined. The braking strength of glass which has a major impact on the head acceleration, however, is not deterministic but depends on production-related micro-cracks on the glass surface as well as on the loading rate.

The aim of the present paper is to show a pragmatic method, how to include the stochastic failure of glass in crash and impact simulations. The methodology includes a fracture mechanical model for the strain rate-dependent failure of glass, the experimental determination of the glass strength for the different areas of a windscreen (surface, edge, and screen-printing area), the statistical evaluation of the experimental data and the computation of a HIC probability distribution by stochastic simulation.

1 INTRODUCTION

In vehicle development, head impact test on a windscreen are common practice to reduce the risk of injury and protect pedestrians. In these tests, a head impactor is shot at different points on the windscreen at up to 40 km/h while the acceleration $a(t)$ acting on the head's COG is measured. A head injury criterion, also known as the HIC value, can be determined from this empirical equation:

$$\mathrm{HIC} = \max\left\{\left[\frac{1}{t_2-t_1}\int_{t_1}^{t_2} a(t)\mathrm{d}t\right]^{2.5}(t_2-t_1)\right\}. \tag{1}$$

Hereby, t_1 and t_2 are the time limits, which have to be chosen in such a way that the HIC value becomes a maximum. In the present application, the maximum time difference is limited to 15 ms which is also known as HIC15. A HIC limit of 1000 indicates that a serious head injury can be expected. Therefore, the goal of vehicle development is not to exceed this value in the head impact test. Numerical simulations play an important role in a modern car development process. It is therefore essential to develop predictable and robust finite element

models for such crash tests. Hereby, important aspects must be considered for head impacts on windscreens. On the one hand, the structure of the windscreen consisting of two layers of glass and a polymer interlayer made of PVB must be reproduced exactly by the FE mesh. On the other hand, constitutive models for the rate-dependent materials PVB and glass must be available. In addition, there is the fact that the breaking strength of glass is not a deterministic value but varies greatly. Consequently, glass strength distribution functions must also be available.

As for the computational treatment of windscreens, various models for laminated glass have been discussed in the literature over the past few decades. In [1] and [2], the extended finite element method (XFEM) was applied to model crack propagation in glass. Furthermore, peridynamics provide a promising approach to describe crack propagation in the glass in detail [3]. Another modelling technique using cohesive zone elements was applied in [4] and [5]. An alternative model using the discrete element method (DEM) can be found in [6].

Due to limitations in computation and meshing time, the previously mentioned models are not used very often in an industrial environment where classical shell elements are preferred, and element erosion is used to approximate crack propagation in a simple but efficient way. However, fracture in such FE simulations is inherently mesh dependent. This disadvantage was addressed by Pyttel et al. [7] and fixed by introducing a non-local method. An enhanced non-local model was proposed by Alter et al. [8]. This model is also used in the present paper and was implemented as user subroutines in the explicit FE-packages Altair RADIOSS and Ansys LS-DYNA.

2 EXPERIMENTAL FINDINGS

2.1 Head Impact Tests

In order to get an overview of the scatter in the event of a head impact, ten brand-new windscreens (Audi A3) were tested using a free-flying head impactor (Euro NCAP adult head). The impactor was shot at 10 m/s in the centre of the four-point supported windscreen. Figure 1 shows three of these tests in comparison. In test (a) the initial fracture starts between 0 and 1 ms, in test (b) between 2 and 3 ms and in test (b) even between 7 and 8 ms. Clearly, the earlier the glass breaks, the softer reacts the glass pane and the lower the risk of head injury. Because of this stochastic fracture behaviour, the HIC15 values vary between 418 and 566 in 10 identical tests [9].

In another study [8], the windscreens (Mercedes Class C) were glued to a wooden frame to approximate the situation in a real car. HIC15 values of 295 to 575 were measured in three head impact tests in the middle of the pane under the same conditions. This shows the high scattering of impact tests on windscreens caused by the stochastic fracture behaviour of glass.

2.2 Stochastic Fracture of Glass

Due to the manufacturing process of windscreens, microcracks occur on the surface of the windscreen and at the edges during handling, transport, silkscreen printing and edge processing. In order to determine the different strengths that occur for these different areas, coaxial ring-on-ring tests were carried out for surface, silkscreen area and PVB side. This test setup can be seen in Figure 2 (left). The round samples were taken from the windscreens using water jet

cutting Since the ring-on-ring test should only be used for flat plates, the specimens were taken out from the screen at positions with low curvature. See [11], [13] for detailed information.

The panes were then separated through a separation of the PVB interlayer. This enabled us to examine the strengths on the surface and on the PVB side separately under controlled loading conditions. For the edges we used four-point-bending tests. Figure *2* (right) shows the corresponding distribution functions for the different areas. From the graphic it can be seen that there are enormous differences in strength within the windscreen. The data was evaluated using a left truncated Weibull distribution

$$P(x) = 1 - \exp\left[\left(\frac{\tau}{\eta}\right)^{\beta} - \left(\frac{x}{\eta}\right)^{\beta}\right]. \tag{2}$$

Hereby η is the scale parameter, β is the shape parameter and τ is the so-called truncation point below which no failure occurs. Using $\tau = 0$ leads to the well-known two-parameter Weibull distribution. Since a single critical crack length in the glass is sufficient to destroy almost the entire load-bearing capacity of the windscreen in the event of a head impact, the weakest link theory and thus the Weibull distribution is an appropriate approach. Details of these experimental investigations can be found in [9]. If the sample areas vary, the probabilities can be regularized according to the area ratio:

$$\sigma_2 = \sigma_1 \left(\frac{A_1}{A_2}\right)^{-\frac{1}{\beta}}. \tag{3}$$

This equation can also be used to regularize different element sizes in FE simulations. Due to manufacturing processes, there is a certain distribution of micro-cracks within the windscreen. When the windscreen is loaded, these microcracks grow with a subcritical velocity until they reach a critical length, causing macroscopic fracture due to instable crack growth. Consequently, failure occurs when the crack reaches a critical length. Thus, the distribution functions for failure stress in Figure 2 (right) are based on critical crack lengths. However, within the unloaded windscreen we have initial microcracks. From this it follows that the crack growth up to the point of fracture must be considered. This can be achieved using the laws of linear elastic fracture mechanics. For subcritical crack growth, the crack velocity can be expressed by the stress intensity

$$K_I = Y\sigma\sqrt{\pi a}, \tag{4}$$

with the current crack length a and the geometry factor Y. In the case of fracture, we obtain the critical stress intensity $K_{IC} = Y\sigma\sqrt{\pi a_f}$, where a_f is the critical crack length. A linear approximation for the transition from subcritical to critical crack growth (failure) can be done by two crack growth parameters n and v_0:

$$v = \frac{da}{dt} = v_0 \left(\frac{K_I}{K_{IC}}\right)^n \tag{5}$$

from which the initial crack length a_i can be computed reversely by integration. Crack growth parameters are dependent on environmental conditions and can be determined experimentally by dynamic fatigue tests, see [11] and the references therein.

Table 1 contains the crack growth parameters for different humidities at a temperature of 25°C.

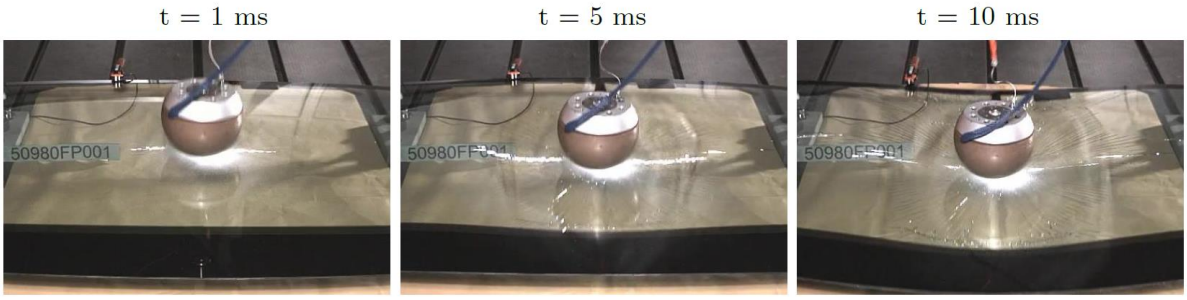

(a) Initial fracture of test number 1 between 0 and 1 ms.

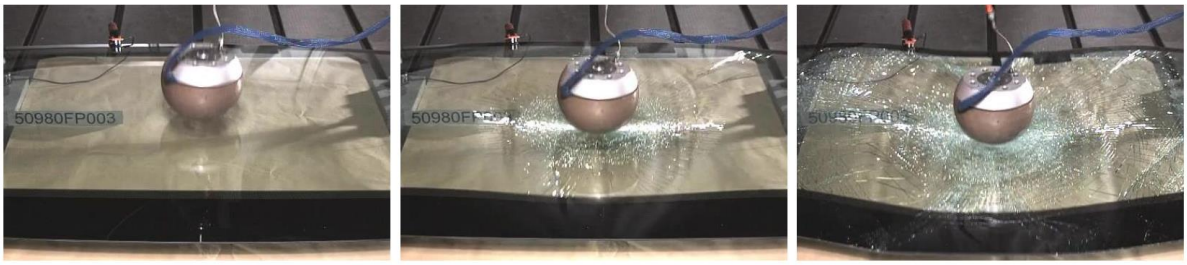

(b) Initial fracture of test number 3 between 2 and 3 ms.

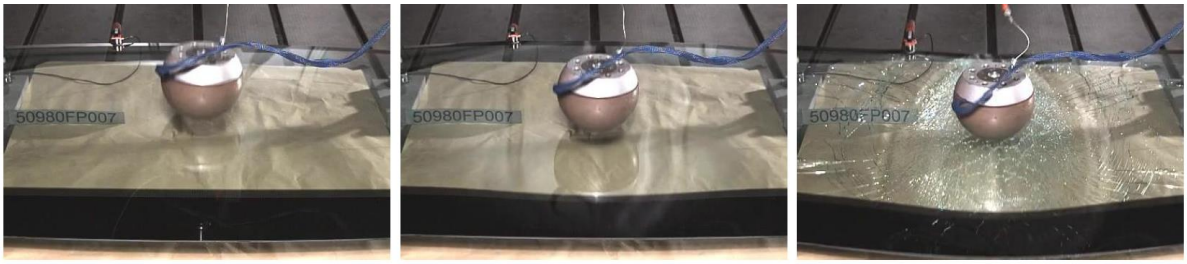

(c) Initial fracture of test number 7 between 8 and 9 ms.

Figure 1: Comparison of head impacts on three windscreens (Audi A3)

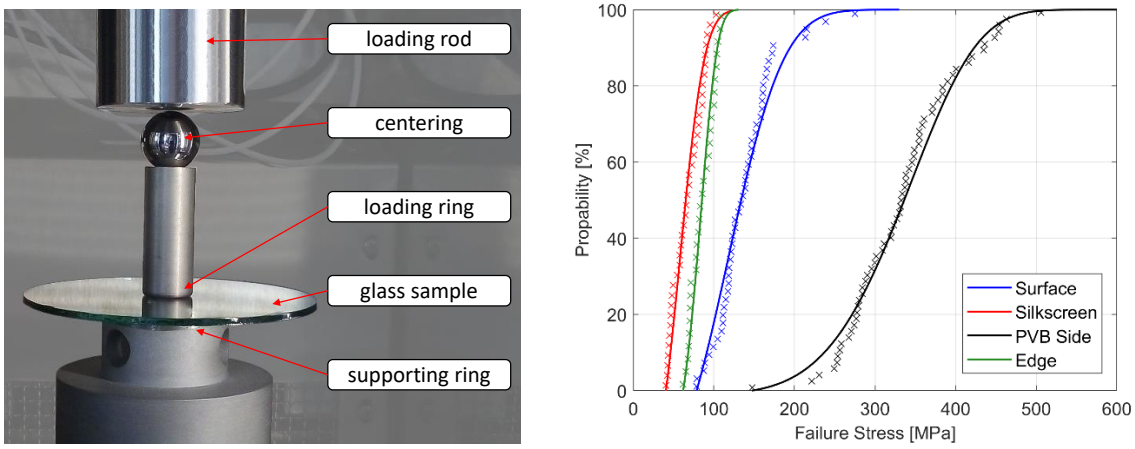

Figure 2: Test setup for the ring-on-ring tests (left) and distribution functions for the different areas (right)

Table 1: Crack growth parameters as a function of humidity

H [%rh], 25°C	30	40	50	60	70
n	15.43	15.10	14.75	12.96	12.26
v_0	9.54	10.22	10.47	13.95	15.99

2.3 Rate Dependency of Glass

As already mentioned in sec. 2.2, cracks start to travel in a subcritical manner with a low velocity under an applied load until the fracture toughness is reached. The velocity of a certain crack depends, among other parameters, on the humidity and the stress intensity. Experimental data could be found in [12]. The behaviour of the subcritical crack growth velocity can be divided into four different regions. In the first region, named "0" in Figure 3 left, no crack velocity can be observed. After a certain value of the stress intensity, cracks start to propagate, and the velocity shows a nearly linear behaviour in a log-log-plot. In region 2, a kind of saturation is reached before the crack starts to propagate in an unstable manner and reaches a maximum velocity of about 1520 m/s.

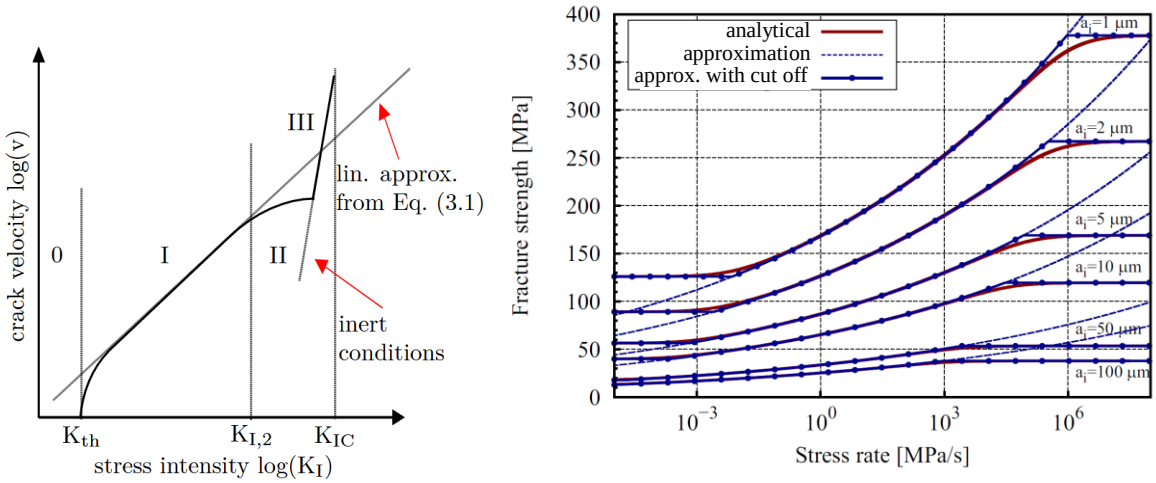

Figure 3: Left: Different regions of subcritical crack growth velocity. Right: Fracture strength as a function of stress rate for different initial crack lengths.

Often the entire range of the subcritical crack growth regime until reaching the fracture toughness is approximated by the region 1 which may be described by the empirical power law shown in eq. (4). Under the assumption of a constant stress rate, a combination of eq. (3) and (4) leads to an approximation of the fracture strength $\sigma_{\mathrm{max,approx}}$ via

$$\sigma_{\mathrm{max,approx}} = \left(\frac{2(\mathrm{n}+1)\mathrm{K_{Ic}^{n}}}{\mathrm{v_0}(\mathrm{n}-2)\left(Y\sqrt{\pi}\right)^{\mathrm{n}}\mathrm{a_i}^{\frac{\mathrm{n}-2}{2}}} \right)^{1/(1+\mathrm{n})} \dot{\sigma}^{1/(1+\mathrm{n})} . \tag{6}$$

Besides the crack growth parameters n and v_0 and the fracture toughness K_{Ic}, the approximated fracture strength depends also on the stress rate $\dot{\sigma}$ and the size of an initial intended flaw a_i. The behaviour is shown for different initial crack lengths in fig. 3 right. As it can be seen, there is no lower or upper bound in the estimation of the fracture strength. As mentioned before, there should be a maximum fracture strength for a certain crack length due to the linear elastic fracture mechanics by reaching the fracture toughness and a lower limit where no crack growth takes place which leads to a lower fracture strength value of

$$\sigma_{\min} = \frac{K_{Th}}{\sqrt{\pi a} Y} \tag{7}$$

and an upper strength value of

$$\sigma_{\max} = \frac{K_{Ic}}{\sqrt{\pi a} Y} \tag{8}$$

An extension of eq. (6) by the cut-off conditions from eq. (7) and (8):

$$\sigma_0 = \min\left(\sigma_{\max}, \max\left(\sigma_{\min}, \sigma_{\max,approx}\right)\right) \tag{9}$$

is shown in fig. 3 right which is used in the current approach. The different initial surface conditions on the different areas of the windscreen are considered internally in the user subroutine whereby a stochastic distribution or a constant initial crack length per area can be chosen.

3 NUMERICAL TREATEMENT

3.1 A Non-Local Material Model for Glass

Since Glass is nearly perfect linear elastic, the material is numerically described by Hooks law. Initial failure of glass is modelled via the extended Equation (6) by the cut-off conditions (7) and (8) using the stress criterion by Rankine. In case of failure, a simple damage approach in accordance with Pyttel et al. [7] is used for a linear stress reduction perpendicular to the failure introducing principal stress. Stress reduction is performed in dependency of the element size and the current time step size to capture the maximum crack growth velocity of glass which is approximately 1520 m/s.
In a real-world application, a crack leads to a stress intensity at the crack tip. Due to rather large elements used in finite element application for the simulation of the head impact, the stress intensity is underestimated by the element erosion. To take care for the stress intensity in the FE approach, a reduction of strength of elements in the direction of a propagating crack in the direct neighbourhood is used

$$\sigma_{0,fin} \begin{cases} \sigma_0 & \text{without neighbouring crack} \\ \sigma_0 / f(l_{el}) & \text{with neighbouring crack} \end{cases} \tag{10}$$

whereby the function for strength reduction $f(l_{el})$ depends on the element size l_{el} and the position of the in-plane integration point.

3.2 Material Modelling of the Interlayer

The polymer interlayer of the windscreen consists of polyvinyl butyral (PVB) which can withstand large deformations and has a very strong strain rate dependency. Tensile tests at different speeds were carried out in order to identify the rate dependency. For material modelling a nearly incompressible hyperelastic model was combined with a viscoelastic model.

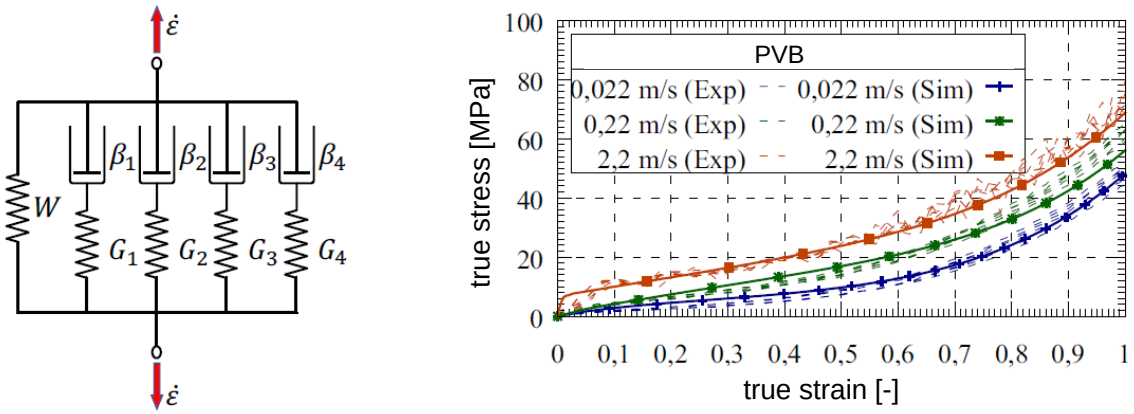

Figure 4: Left: Rheological model. Right: Validation of the model using highspeed tensile tests.

Figure 4 left shows the rheological model which consists of a hyperelastic spring and a series of four Maxwell elements. The deviatoric part of the hyperelastic model is given by the following strain energy function:

$$\mathrm{W}_{\mathrm{DEV}}(\mathrm{I}_C, \mathrm{II}_C) = \sum_{i,j=0}^{n} A_{ij}(\mathrm{I}_C - 3)^i(\mathrm{II}_C - 3)^j, \tag{11}$$

where A_{ij} are material constants and $\mathrm{I}_C, \mathrm{II}_C$ are the first and second invariant of the right Cauchy-Green tensor. All parameters of the material model were identified numerically using the optimization tool LS-OPT. The numerical results are in a good agreement with the experiments, see Figure 4 right.

3.3 Assembling of the FE model

For discretization of the windscreen, a shared shell-solid-shell approach with a regular mesh is used. Thereby, fully integrated shell elements for the glass plates combined with solid elements for the PVB interlayer are used. In order to get the physical composition and thus the correct flexural stiffness as well as stress prediction, the shell mid surfaces as well as the contact thicknesses are shifted to the outer sides by a half of the ply thicknesses. Shear coupling is realized by merging the nodes of the shells and the solid elements, see Figure 5. Delamination effects are not considered as a result. A validated commercial model of the impactor was used.

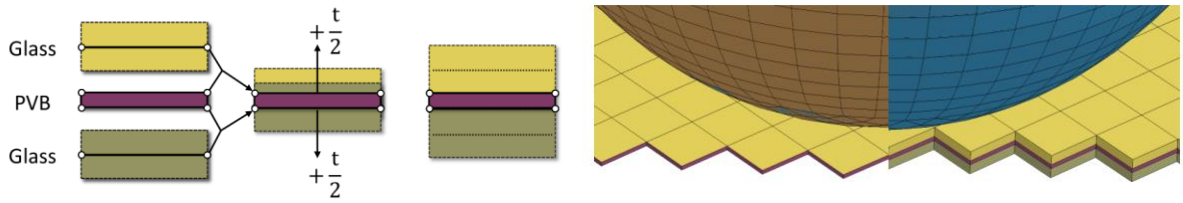

Figure 5: Left: Modelling technique for LSG using shared node approach. Right: Visualization of the shifted shell thicknesses together with a part of the head impactor model.

3.4 Head Impact Simulation

The basic validation of the discretization and the failure modelling were done by head impact tests on Mercedes Class C windscreens with constant crack lengths for different areas, means without a stochastic approach. The initial crack sizes were assumed to be $a_i = 1\ \mu m$ for the air surface, $a_i = 0.4\ \mu m$ for the laminated and thus protected surface and $a_i = 5\ \mu m$ for the edges of the windscreen. Additionally, it is assumed, that the PVB-interlayer protects the inner surface from water vapor, the main cause of subcritical crack growth effects, and thus the rate dependency of fracture strength is neglected for the surfaces concerned. A comparison of the measured and the predicted acceleration curves as well as the fracture pattern shows that the proposed approach is basically capable to represent all different stages of fracture of the windscreen. No significant influence of the element formulation (reduced or fully integrated) as well as of the through thickness integration rule could be identified. A convergence study with average element sizes of 10 mm, 5 mm and 2.5 mm was performed additionally to show the mesh independency of the non-local model.

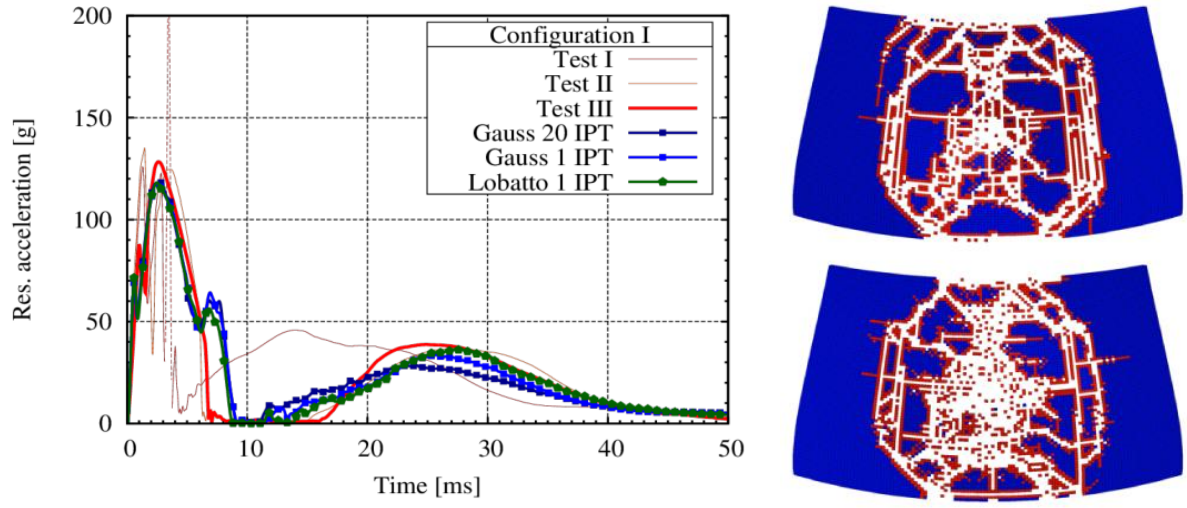

Figure 6: Left: Resultant acceleration of three different test in comparison to predicted acceleration curves using different numbers of in-plane integration points and different integration rules. Right: Predicted fracture pattern for the outer glass pane (top) and the lower glass pane (bottom).

3.5 Stochastic Simulation

To consider the stochastic fracture behaviour of glass in the simulation, the corresponding distribution functions in Figure 2 must be transferred separately for edges, each side of the surface and screen-printing area to the material model for glass. However, these distribution functions are based on critical crack lengths. Therefore, we compute the initial crack lengths a_{in} in a first step using Equation (5). These crack lengths are then randomly distributed across the windscreen model for each Gauss point. Hereby, the different element sizes must be considered using Equation (3).
If the glass ply is loaded, the initial cracks grow subcritically when a threshold value of the stress intensity $K_{I,th}$ is exceeded. Only when a critical crack size is reached, macroscopic fracture occurs. This can be described by the critical stress intensity K_{IC}. This subcritical crack growth can again be described by Equation (5) using the algorithm in shown in Figure 7. If σ_{fail} is reached a macroscopic failure occurs. This is modelled with the present non-local model using the element erosion technique, i.e., the stiffness of the corresponding element is set to zero in the time it takes for the crack to propagate through the element.

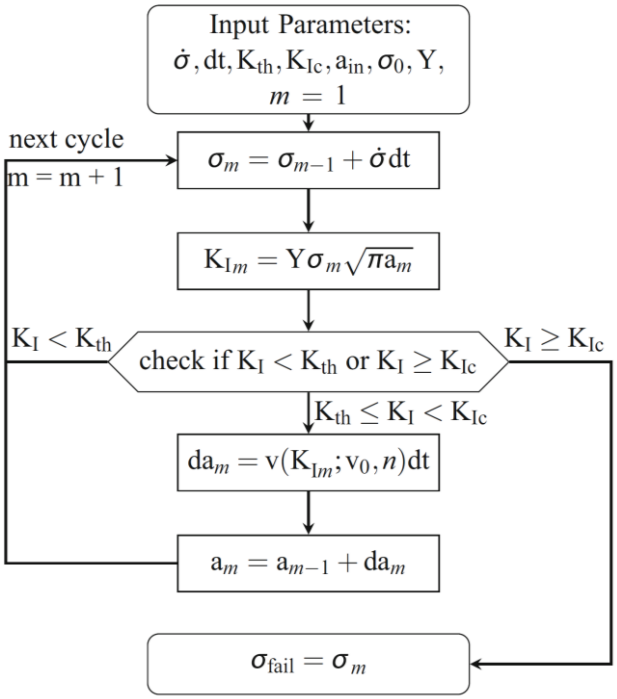

Figure 7: Algorithm for subcritical crack growth to failure

For the stochastic simulation we repeat this process many times. For the following frequency distributions, 250 head impact simulations each with randomly distributed initial cracks were carried out. We examined two different boundary conditions: A simple four point supported windscreen and an elastic support close-to-the-car where the windscreen was glued to a wooden frame using windscreen adhesive.

The experimental and numerical HIC values for the four-point supported windscreen are

shown in Figure 8. Most HIC values for the chosen test setup are accumulating at the upper bound. A putative normal distribution of head injury values is calculated between approximately 400 and 520. Five of ten experimental values are within this range, while the other five values are at the upper bound. It can therefore be assumed that the stochastic fracture model can reproduce the real head impact tests realistically.

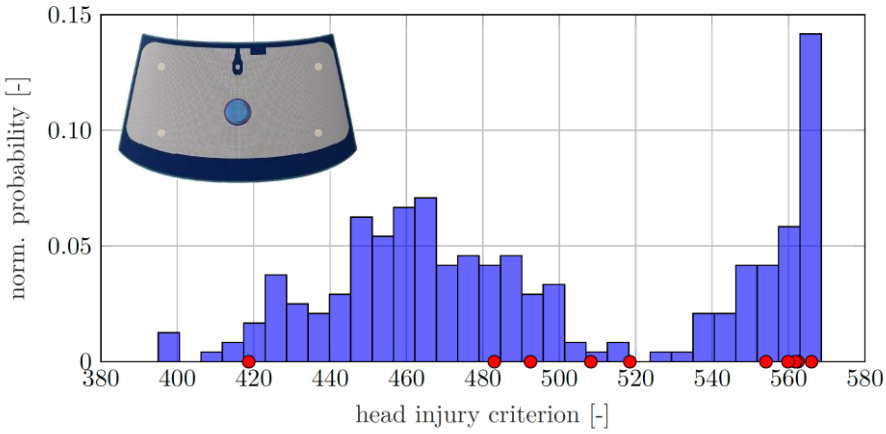

Figure 8: HIC probability for head impact tests on four-point supported windscreens. Ten experimentally determined values (red dots) and 250 values from stochastic simulations are depicted

As a next step we show a purely numerical study where the windscreen was glued to a wooden frame. Details of the model can be found in [9]. Figure 9 shows the numerically predicted HIC values calculated by Equation (1). The values are scattered between 411.74 and 1292.01. An accumulation around HIC = 480 can be observed. 1.6 % of the calculated values are higher than 1000. The calculated values are like the values from literature in respect of the statistical range. No freely available database for the stochastic scatter of the pedestrian head impact could be found. This is complicated by the manufacturing-dependent, nonmaterial-specific strength of glass. As a result, each manufacturing line generates its own glass strength distribution and thus its own HIC distribution for a certain windscreen.

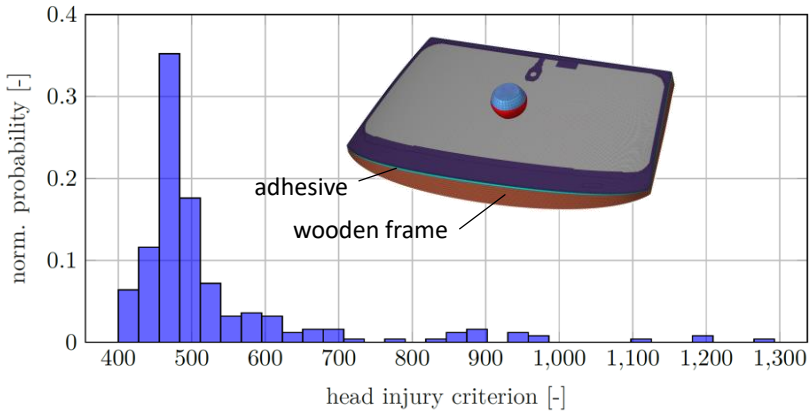

Figure 9: HIC probability for head impact simulations on windscreens glued on a wooden frame. 250 HIC values from stochastic simulations are depicted

4 CONCLUSIONS AND OUTLOOK

In the present paper, a methodology was proposed to consider the stochastic fracture behaviour of glass in the numerical simulation. This includes both the required experimental work and the numerical implementation for FE simulation. To determine the glass strength distribution, all areas of the windshield must be examined separately. These are the glass surfaces, the edge, and the screen-printed area using ring-on ring tests and four-point bending tests respectively. With these distribution functions the production-related initial cracks can be computed reversely, and subcritical crack growth can be considered using fracture mechanics. Using stochastic simulation, trends can then be shown that would otherwise not be possible due to the limited number of real tests. However, the predictive ability of the simulation is heavily dependent on the precise modelling of the fracture behaviour of glass. Therefore, detailed work on the post-fracture behaviour of laminated glass will be subject of future investigations.

REFERENCES

[1] J. Xu et al.: Characteristics of windscreen cracking upon low-speed impact: numerical simulation based on the extended finite element method, Computational Materials Science (2010) **48**(3):582-588.

[2] X. Xu, B. Liu, Y. Li: Investigation on Dynamic Propagation Characteristics of In-Plane Cracks in PVB Laminated Glass Plates. Advances in Materials Science and Engineering (2016) 10.1155/2016/1468390.

[3] K. Naumenko, M. Pander, M. Würkner: Damage patterns in float glass plates: Experiments and peridynamics analysis. Theoretical and Applied Fracture Mechanics (2022) **118**:103264.

[4] S. Chen et al.: Finite element modelling of impact damage in polyvinyl butyral laminated glass, Composite Structures (2016) **138**:1-11.

[5] D. Lin et al.: Numerical simulations of impact fracture behavior of an automotive windscreen glazing: An intrinsic cohesive approach. Composite Structures (2017) **186**:79-93.

[6] W. Xu, M. Zang, Four-point combined DE/FE algorithm for brittle fracture analysis of laminated glass, International Journal of Solids and Structures (2014) **51**(10):1890-1900.

[7] T. Pyttel, H. Liebertz, J. Cai: Failure criterion for laminated glass under impact loading and its application in finite element simulation, International Journal of Impact Engineering (2011) **38**(4):252-263.

[8] C. Alter, S. Kolling, J. Schneider: An enhanced non-local failure criterion for laminated glass under low velocity impact. International Journal of Impact Engineering (2017) **109**:342-353.

[9] C. Brokmann: A Model for the stochastic fracture behavior of glass and its application to the head impact on automotive windscreens. Springer (2022).

[10] S. Müller-Braun et al.: Strength of the individual glasses of curved, annealed and laminated glass used in automotive windscreens, Engineering Failure Analysis (2021) **123:**105281.

[11] C. Brokmann, S. Kolling, J. Schneider: Subcritical crack growth parameters in glass as a

function of environmental conditions. Glass Structures & Engineering (2021) **6**:89-101.
[12] S. M. Wiederhorn: Influence of water vapor on crack propagation in soda-lime glass. Journal of the American Ceramic Society 50.8 (1967): 407-414.
[13] S. Müller-Braun, J. Schneider: Biaxially curved glass with large radii—determination of strength using the coaxial double ring test. Glass Structures & Engineering 2.2 (2017): 121-131.